Cellular/Molecular

Stabilization of Spine Synaptopodin by mGluR1 Is Required for mGluR-LTD

Luisa Speranza,[1] Yanis Inglebert,[2] Claudia De Sanctis,[1] Pei You Wu,[2] Magdalena Kalinowska,[1] R. Anne McKinney,[2*] and Anna Francesconi[1*]

[1]Dominick P. Purpura Department of Neuroscience, Albert Einstein College of Medicine, New York, New York 10461, and [2]Department of Pharmacology & Therapeutics, McGill University, Montreal, QC H3G 0B1, Canada

Dendritic spines, actin-rich protrusions forming the postsynaptic sites of excitatory synapses, undergo activity-dependent molecular and structural remodeling. Activation of Group 1 metabotropic glutamate receptors (mGluR1 and mGluR5) by synaptic or pharmacological stimulation, induces LTD, but whether this is accompanied with spine elimination remains unresolved. A subset of telencephalic mushroom spines contains the spine apparatus (SA), an enigmatic organelle composed of stacks of smooth endoplasmic reticulum, whose formation depends on the expression of the actin-bundling protein Synaptopodin. Allocation of Synaptopodin to spines appears governed by cell-intrinsic mechanisms as the relative frequency of spines harboring Synaptopodin is conserved *in vivo* and *in vitro*. Here we show that expression of Synaptopodin/SA in spines is required for induction of mGluR-LTD at Schaffer collateral-CA1 synapses of male mice. Post-mGluR-LTD, mushroom spines lacking Synaptopodin/SA are selectively lost, whereas spines harboring it are preserved. This process, dependent on activation of mGluR1 but not mGluR5, is conserved in mature mouse neurons and rat neurons of both sexes. Mechanistically, we find that mGluR1 supports physical retention of Synaptopodin within excitatory spine synapses during LTD while triggering lysosome-dependent degradation of the protein residing in dendritic shafts. Together, these results reveal a cellular mechanism, dependent on mGluR1, which enables selective preservation of stronger spines containing Synaptopodin/SA while eliminating weaker ones and potentially countering spurious strengthening by *de novo* recruitment of Synaptopodin. Overall, our results identify spines with Synaptopodin/SA as the locus of mGluR-LTD and underscore the importance of the molecular microanatomy of spines in synaptic plasticity.

Key words: **dendritic spines; mGluR-LTD; mGluR1; protein turnover; spine apparatus; Synaptopodin**

Significance Statement

Long-term changes in functional synaptic strength are associated with modification of synaptic connectivity through stabilization or elimination of dendritic spines, the postsynaptic locus of excitatory synapses. How heterogeneous spine microanatomy instructs spine remodeling after long-term synaptic depression (LTD) remains unclear. Metabotropic glutamate receptors mGluR1 and mGluR5 induce a form of LTD critical to circuit function in physiological and disease conditions. Our results identify spines containing the protein Synaptopodin, which enables local assembly of a spine apparatus, as the locus of expression of mGluR-LTD and demonstrate a specific role of mGluR1 in promoting selective loss after mGluR-LTD of mature dendritic spines lacking Synaptopodin/spine apparatus. These findings highlight the fundamental contribution of spine microanatomy in selectively enabling functional and structural plasticity.

Received July 17, 2021; revised Jan. 7, 2022; accepted Jan. 10, 2022.

Author contributions: L.S., R.A.M., and A.F. designed research; L.S., Y.I., C.D.S., P.Y.W., and M.K. performed research; L.S., Y.I., C.D.S., P.Y.W., M.K., R.A.M., and A.F. analyzed data; R.A.M. and A.F. wrote the paper.

This work was supported by National Institute of Mental Health R01MH108614 to A.F.; Canadian Institutes of Health Research MOP 86724 to R.A.M.; and the Norman Zavalkoff Family Foundation to R.A.M. We acknowledge the assistance of the Neural Cell Engineering and Imaging Core of the Einstein Rose F. Kennedy Intellectual and Developmental Disabilities Research Center supported by National Institute of Child Health and Human Development U54 HD090260, and of the Analytical Imaging Facility at Albert Einstein College of Medicine partly funded by National Cancer Institute Cancer Center Grant P30CA013330. We thank members of the A.F. and R.A.M. laboratories for comments on the manuscript; and Francois Charron for excellent technical assistance.

*R.A.M. and A.F. are joint senior authors.

The authors declare no competing financial interests.

Correspondence should be addressed to Anna Francesconi at anna.francesconi@einsteinmed.edu or R. Anne McKinney at anne.mckinney@mcgill.ca.

https://doi.org/10.1523/JNEUROSCI.1466-21.2022

Introduction

Dendritic spines, small protrusions on excitatory neurons, serve as the sites for structural changes during long-term changes in synaptic strength. The mechanisms of LTP associated with spine outgrowth and enlargement (Harris, 2020) are well understood, whereas the occurrence of structural changes in spines after LTD is more controversial and the underlying mechanisms not fully understood (Stein and Zito, 2019). In some incidences, spines are eliminated or reduced in size after LTD, but in other cases synaptic weakening can occur independently of spine shrinkage (Wang et al., 2007; Thomazeau et al., 2021). This complexity is compounded by the heterogeneous microanatomy of spines (Berry and Nedivi, 2017), with some marked by transient or

enduring presence of smooth endoplasmic reticulum (sER) (Spacek and Harris, 1997; Perez-Alvarez et al., 2020). In telencephalic regions, a subset of large spines contain a spine apparatus (SA) (Spacek, 1985; Spacek and Harris, 1997), a poorly understood neuron-specific sER organelle that supports local Ca^{2+} storage (Fifková et al., 1983; Korkotian et al., 2014). The SA, which is present in ~10%-20% of adult hippocampal and cortical mature spines (Spacek and Harris, 1997), is made of stacks of sER tubules intercalated with F-actin and Synaptopodin (Synpo), an F-actin-bundling protein (Deller et al., 2000; Asanuma et al., 2005). Synpo is necessary and sufficient for the formation and maintenance of the SA, as shown by absence of the organelle in mice lacking Synpo (Deller et al., 2003). At present, the contribution of the SA to forms of activity-dependent synaptic plasticity is incompletely understood, and the mechanisms underlying enduring presence of Synpo in subsets of dendritic spines remain unclear.

Activation of group 1 metabotropic glutamate receptors (Gp1 mGluRs), mGluR1 and mGluR5, by synaptic or pharmacological stimulation, induces LTD at Schaffer collateral (SC)-CA1 synapses (mGluR-LTD) (Lüscher and Huber, 2010), a form of plasticity altered in many neurodevelopmental disorders (Huber et al., 2002; Sahin and Sur, 2015). It was further shown that the capacity of Gp1 mGluRs to depress synaptic transmission relies on sER (Holbro et al., 2009), but whether presence of Synpo is needed for mGluR-LTD to occur is untested. Gp1 mGluRs are critical to circuit refinement during development, and their activation was shown to be required for activity-dependent shrinkage of large spines (Oh et al., 2013) and heterosynaptic structural plasticity (Oh et al., 2015). Nevertheless, the impact of mGluR-LTD on spine elimination was recently questioned, since contrasting observations have reported either spine loss induced by mGluR-LTD (Ramiro-Cortés and Israely, 2013; Wiegert and Oertner, 2013) or lack of effect on spine density (Thomazeau et al., 2021). Moreover, whether spines containing the SA undergo structural remodeling during mGluR-LTD is unknown.

Here we show that expression of Synpo/SA in spines is required for induction of mGluR-LTD at hippocampal SC-CA1 synapses. We find that mGluR-LTD induces selective loss of mushroom spines that do not contain Synpo, an effect mediated by mGluR1. We further report that mGluR-LTD triggers selective degradation of Synpo in dendritic shafts via the lysosomal pathway, whereas Synpo at spine synapses is stabilized through association with mGluR1. Together, these findings uncover a novel cellular mechanism dependent on mGluR1 that enables selective preservation of spines containing the SA while eliminating weaker ones.

Materials and Methods

Animals. All procedures were according to protocols approved by the Albert Einstein College of Medicine, in accordance with the *Guide for the care and use of laboratory animals* by the United States PHS or the guidelines of the Canadian Council on Animal Care and the McGill University Comparative Medicine and Animal Resources animal handling protocols 5057. Sprague Dawley rats were used for primary neuronal cultures. *Grm1* KO mice ($Grm1^{KO}$) (Mende et al., 2016) and *Synpo* KO mice (Deller et al., 2003) crossed with L15 GFP-expressing mice used as WT (Verbich et al., 2016) were previously described. Mice were fed *ad libitum* and housed with a 12 h light/dark cycle. *Synpo* KO or L15 male mice and $Grm1^{KO}$ or $Grm1^{WT}$ mice of both sexes were used for experiments.

Electrophysiology. Hippocampal slices were obtained from P30-P40 old *Synpo* KO or L15 mice. Mice were deeply anesthetized with isoflurane and killed by decapitation. Slices (400 μm) were cut on a vibratome (Leica Microsystems, VT1200S) in a sucrose-based solution containing the following (in mM): 280 sucrose, 26 $NaHCO_3$, 10 glucose, 1.3 KCl, 1 $CaCl_2$, and 10 $MgCl_2$ and were transferred at 32°C in regular ACSF containing the following (in mM): 124 NaCl, 5 KCl, 1.25 NaH_2PO_4, 2 $MgSO_4$, 26 NaHCO3, 2 $CaCl_2$, and 10 glucose saturated with 95% O_2/5% CO_2 (pH 7.3, 300 mOsm) for 15 min before resting at room temperature (RT) for 1 h in oxygenated (95% O_2/5% CO_2) ACSF. For recording, slices were transferred to a temperature-controlled (32°C) chamber with oxygenated ACSF. To assess mGluR-LTD, slices were placed into a heated (32°C) recording chamber of an upright microscope (DM LFSA Microsystems) and perfused continuously with regular ACSF. Field excitatory postsynaptic potentials (fEPSPs) were recorded in the *stratum radiatum* of the CA1 region by using glass microelectrodes filled with 3 M NaCl. $GABA_A$ receptor-mediated inhibition was blocked with 100 μM picrotoxin, and the area CA1 was surgically isolated from CA3 to avoid epileptiform activity. fEPSPs were elicited at 0.1 Hz by a digital stimulator that fed by a stimulation isolator unit. All data analyses were performed with custom-written software in Igor Pro 8 (Wavemetrics). fEPSP slope was measured as an index of synaptic strength.

Immunohistochemistry. Hippocampal slices of 100 μm were obtained from P30 to P40 old L15-$Synpo^{KO}$ or L15 mice. The slices were incubated in ACSF at RT for 1 h before treatment with *RS*-DHPG (100 μM) for 5 min or control. Following treatment, the slices were fixed in 0.1 M PB containing 4% PFA, pH 7.4, overnight at 4°C. After fixation, slices were washed in 0.1 M PB, permeabilized in 0.4% Triton X-100, and blocked with 1.5% heat-inactivated horse serum overnight at 4°C. Slices were incubated with primary anti-Synpo antibody (1:500) in permeabilizing solution for 3 d at 4°C, washed with PB, and incubated with anti-rabbit secondary antibody conjugated to DyLight 649 (1:500; Jackson ImmunoResearch Laboratories) for 3 h, washed, and mounted with DAKO Fluorescent Mounting medium (Dako Canada) onto microscope slides before imaging and subsequent blinded analysis. Spine images were taken in *z* stacks using a Leica Microsystems SP8 confocal microscope with oil-immersion 63× objective at 6× zoom-in. The images were deconvolved and analyzed using software Huygens and Imaris, respectively.

Neuronal cultures and drug treatments. Hippocampi and cortices from newborn rat pups dissected in Ca^{2+}/Mg^{2+}-free HBSS were digested with 0.25% trypsin and DNase (2000 U/ml) for 20 min at 37°C and mechanically triturated. Viable cells, determined by trypan blue dye exclusion, were plated at 8×10^4/1.13 cm^2 on poly-L-lysine-coated cover glasses and at 2.5×10^5/1.9 cm^2 in multiwell plates. Cells were maintained at 37°C, 5% CO_2 in serum-free Neurobasal A medium with 2% B-27 supplement, 2 mM GlutaMax (from Invitrogen), penicillin (50 U/ml), and streptomycin (50 μm/ml). After 5 DIV, a mix of 37 mM uridine and 27 mM 5-fluoro-2-deoxyuridine was added; half medium was replaced weekly and neurons used at 19-21 DIV.

For chemical mGluR-LTD, cells were rinsed with prewarmed medium and treated with 50 μM *S*-DHPG (Tocris Bioscience) or vehicle for 15 min at 37°C: cells were rinsed with prewarmed medium and incubated with fresh medium for 30 or 120 min at 37°C. Bay 36-7620 (Bay) or 2-methyl-6-(phenylethynyl) pyridine (MPEP, Tocris Bioscience) was applied alone for 15 min at 37°C or together with DHPG and added to the fresh medium during recovery. For treatment with MG132 (ApexBio), leupeptin or bafilomycin A_1 ($BafA_1$; Sigma-Aldrich), after rinsing with prewarmed medium, drugs or respective vehicle were applied alone in fresh medium for 15 min at 37°C or together with DHPG, and added to fresh medium during recovery. For treatment with rapamycin (Cayman Chemical) or cycloheximide (Sigma-Aldrich), cells were rinsed with prewarmed medium and drugs or vehicle applied in fresh medium for the indicated times at 37°C. After treatments, cells were placed on ice and processed for downstream analysis.

$DiIC_{18}$ labeling. Cells and tissue sections were labeled with the fluorescent dye 1,1′-dioctadecyl-3,3,3′,3′-tetramethylindotricarbocyanine iodide ($DiIC_{18}$; Invitrogen, crystals catalog #D3911) as described previously (Cheng et al., 2014). Briefly, cells plated on cover glasses were fixed with 4% PFA for 10 min and washed with PB. After PB aspiration, $DiIC_{18}$ crystals (3-4 crystals/well) were sprinkled over the cells with an 18 gauge needle. To prevent dehydration, PB was added to the wells and

the plate incubated for 10 min on an orbital shaker at RT protected from light. After washing with PB to remove the crystals, cells were incubated in PB overnight at RT and washed 3 times with PB (5 min per wash) before immunolabeling or mounting on glass slides. For tissue sections, mice were anesthetized with isoflurane and perfused with 4% PFA: the brain was removed and postfixed with 4% PFA overnight at 4°C. After three 5 min washes with PB, 150- or 300-μm-thick coronal sections were cut with a vibratome (Leica Microsystems, VT1000S). The tissue was gently unfolded with a paintbrush and crystals of $DiIC_{18}$ applied with a needle onto the ROIs (parietal and prefrontal cortex). Labeled tissue sections were incubated at 4°C in PB, protected from light, for 7-10 d before image acquisition. For combined tissue immunofluorescence, 50-μm-thick sections incubated with $DiIC_{18}$ for 10 d were pretreated for 30 min at RT with digitonin 100 μg/ml in 3% BSA in PB followed by incubation for 12 h at 4°C with rabbit anti-Synpo (1:400) diluted in digitonin solution. The tissue sections were washed 3 times with PB (5 min each) and incubated with anti-rabbit secondary antibody conjugated to AlexaFluor-488 for 3 h at RT, washed with PB, and mounted on glass slides with ProLong (Cell Signaling Technology).

Immunofluorescence. Cells were rinsed in PB for 2 min and fixed in 4% PFA for 10 min at RT. After permeabilization with 0.1% Triton X-100 in PB for 15 min, cells were incubated for 1 h at RT with blocking solution of either 5% BSA or 5% normal serum. Primary antibodies in blocking solution were applied overnight at 4°C. After three washes with PB for 3 min, cells were incubated for 1-2 h at RT with fluorophore-conjugated secondary antibodies, washed 3 times with PB and mounted on glass slides with ProLong. To label surface AMPARs, cells were rinsed 2 times with prewarmed medium and incubated for 30 min at 37°C with rabbit anti-GluA1 (1:150; Calbiochem/Millipore, RRID:AB_564636) in culture medium. After incubation with anti-GluA1, cells were treated with 50 μM DHPG or vehicle for 15 min at 37°C, rinsed with prewarmed medium, and incubated with fresh medium for 30 min at 37°C. Cells were then washed with PB containing 1 mM $MgCl_2$, 0.1 mM $CaCl_2$ and fixed with 4% PFA for 10 min. After fixation, cells were washed with PB (3 × 5 min), incubated with 5% BSA for 1 h at RT and with secondary fluorescent antibody for 1 h at RT. After washing with PB, cells were permeabilized, blocked, and incubated with primary antibodies as above. The following antibodies were used: rabbit anti-Synpo (1:500; Synaptic Systems, RRID:AB_887825), guinea pig anti-Synpo (1:500; Synaptic Systems, RRID:AB_10549419) chicken anti-MAP2 (1:500; PhosphoSolutions, RRID:AB_2138173), and rabbit anti-mGluR1 (1:2000; RRID:AB_2571735). The following secondary antibodies were used: donkey anti-mouse or rabbit conjugated to AlexaFluor-488 and AlexaFluor-647, goat anti-guinea pig AlexaFluor-488 (Invitrogen), donkey anti-chicken IgY conjugated to AlexaFluor-647 and aminomethylcoumarin acetate (Jackson ImmunoResearch Laboratories).

Microscopy. Wide field fluorescence imaging was conducted with an Olympus IX81 inverted microscope equipped with digital CCD ORCA-R2 camera (Hamamatsu) using 40× (NA = 1.3) or 60× (NA = 1.35) oil objectives. Confocal images were acquired with a Carl Zeiss LSM880 Airyscan using a Plan-Apochromat 63× (NA = 1.4) oil immersion objective; a 561 nm diode pumped solid-state laser (DPSS 561-10) was used to visualize $DiIC_{18}$. Images at 1024 × 1024 pixel resolution were acquired with scan speed set at 6 and pinhole configured to 1 Airy unit for each channel. Stacks of images were acquired with a 0.5 μm Z step and reconstructed with the Fiji's Stacks Z Project function to generate Z-stack projections of the maximum intensity. Images of tissue sections labeled with $DiIC_{18}$ and anti-Synpo were acquired with a Leica Microsystems SP5 Confocal microscope using a 63× (NA = 1.4) oil objective (at 3 or 4× zoom-in).

Image analysis. Analysis was conducted blind to treatment/genotype using the image-processing platform Fiji (Schindelin et al., 2012). To quantify Synpo clusters, a mask of the outline of neurons was generated using MAP2 signal overlay. After background subtraction, individual clusters within the masked region were measured by automated count using the Analyze Particles function on thresholded images. For spine analysis, dendrites and dendritic protrusions were outlined and measured with the segmented line tool. Proximal dendritic segments (~100 μm) were analyzed in both primary and secondary dendrites. Spine density is expressed as number of spines per 10 μm of dendritic length. To classify dendritic spines, the length (l), head width (h), and neck width (n) were manually traced for individual dendritic protrusions. Spine length was measured from the emerging point on the shaft to the tip of spine head, and head diameter was measured at the point of maximum width. Dendritic protrusions were classified according to established morphologic criteria (Harris et al., 1992; Zagrebelsky et al., 2005) and defined as mushroom spines when $h \gg n$ ($h/n > 1.5$) and thin spines when $l > 1$ μm and $h/n \leq 1.5$. Stubby spines and filopodia were rarely observed in the mature primary neurons used in the study and not included in the analysis. For colocalization analysis of Synpo with mGluR1, after background subtraction, the total puncta labeled by the respective antibody were counted with the Fiji Cell_Counter plugin and validated with a secondary analysis using threshold adjustment and the Analyze_Particle plugin for automated counts. A Color-merge channel was then generated and the colocalizing puncta quantified with Cell_Counter and validated with the Coloc2 plugin.

Western blot and immunoprecipitation. Drug-treated cortical neurons were placed on ice, rinsed with ice-cold PB, and lysed in buffer of 20 mM MOPS, pH 7.2, 2 mM EGTA, 5 mM EDTA, 1% Triton X-100 supplemented with a cocktail of protease and phosphatase inhibitors. Cells were incubated on ice for 5 min, scraped off the wells, and collected by centrifugation at 21,000 × g at 4°C for 15 min. Equal amounts of proteins were resolved by SDS-PAGE and processed by Western blot assay per standard protocols using HRP-conjugated secondary antibodies and ECL for detection on film or with an Azure c600 imaging system (Azure Biosystems). The following primary antibodies were used: rabbit anti-Synpo (1:1000), goat anti-Synpo (1:200; Santa Cruz Biotechnology, RRID:AB_2201166), rabbit mGluR1 (1:500, Alomone Labs, RRID:AB_2039984; 1:10 000, RRID:AB_2571736), rabbit anti-pan actin (1:1000; Cell Signaling Technology, RRID:AB_10998774), mouse anti-PSD95 (1:400; Antibodies, RRID:AB_2292909), and mouse anti-γ-tubulin (1:2500; Sigma-Aldrich, RRID:AB_477584).

For immunoprecipitation, brain cortices of adult mice were homogenized on ice in a buffer of 20 mM Tris-HCl, 5 mM EDTA, 100 mM NaCl, 1% Triton X-100, 0.5% sodium deoxycholate (pH 7.4; 10 μl/mg tissue), supplemented with cocktails of protease and phosphatase inhibitors. The tissue was manually homogenized on ice, centrifuged at 13,000 × g for 20 min at 4°C, and supernatant collected. Equal amounts of protein were incubated overnight at 4°C with primary antibodies (rabbit anti-Synpo 3 μl/mg; rabbit anti-mGluR1 RRID:AB_2571736 4 μl/Ip; mouse anti-PSD95 0.9 μg/Ip) or respective control IgG coupled to Protein G-coupled magnetic beads (Dynabeads, Invitrogen). Unbound material was removed, and the beads washed 3 times with homogenization buffer, 3 times with PBS/0.1% Triton X-100, and 1 time with PBS before elution in denaturing sample buffer at 95°C for 5 min.

Statistical analysis. Unless noted, values were imported into Prism 8.1 (GraphPad) for the generation of graphs and statistical tests. Data are reported as mean ± SEM unless indicated: normality and data distribution were assessed with the Kolmogorov–Smirnov test. Two-tailed Student's t test was used to compare two groups and Mann–Whitney test used for nonparametric analysis of ranks when appropriate. One-way ANOVA with Tukey's *post hoc* test was used to compare multiple groups. Gardner–Altman estimation plots used to display spine data and the two-sided permutation t test were generated with the web application estimationstats.com (Ho et al., 2019). $p < 0.05$ was considered significant in all statistical comparisons.

Results

Spines with Synpo are required for mGluR-LTD

Dendritic spines are the sites of excitatory synapses, and their structural and functional properties are modified in response to activity patterns that produce long-term changes in synaptic transmission. Low-frequency stimulation was shown to selectively induce depression of evoked EPSCs in dendritic spines containing sER, an effect that was blocked by Gp1 mGluR antagonists (Holbro et al., 2009). Although this finding suggested that

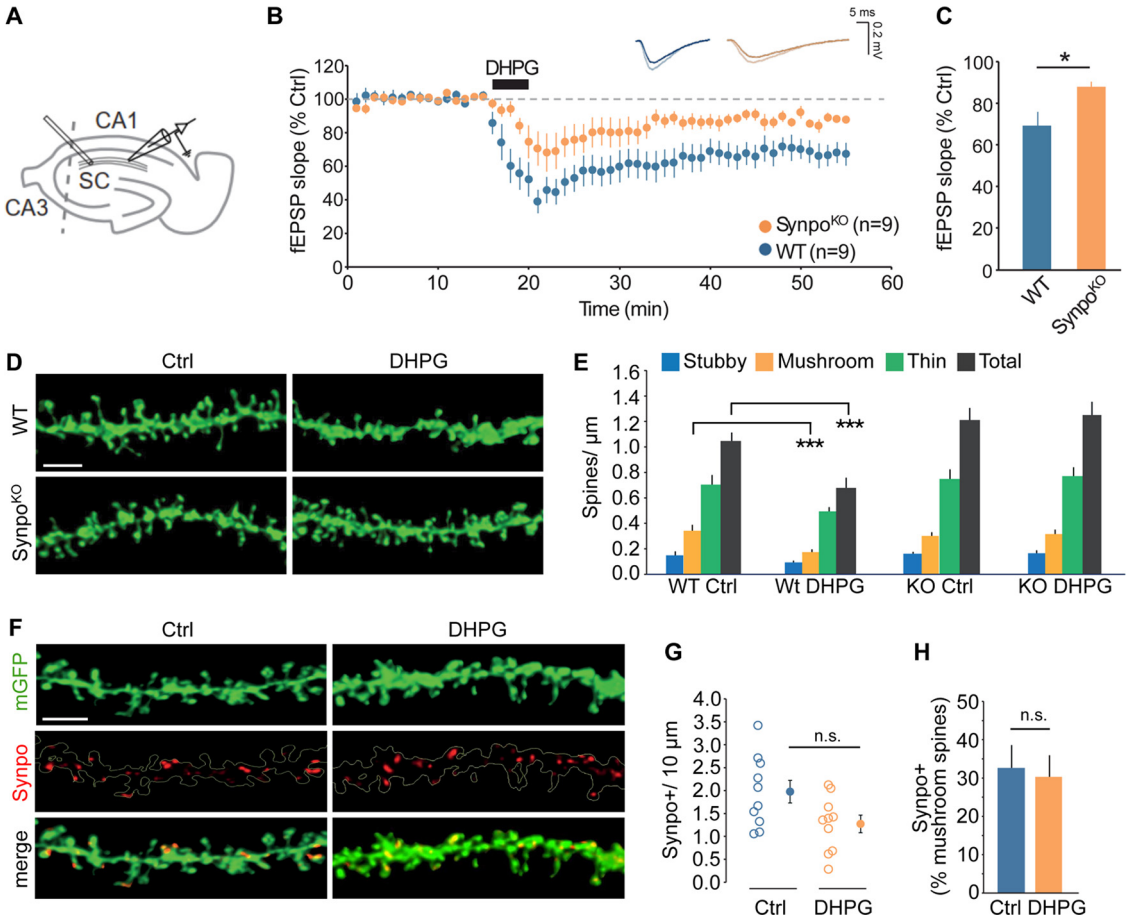

Figure 1. Spines with stable Synpo are required for mGluR-LTD. ***A***, Illustration of the approximate locations of stimulating and recording electrodes in hippocampal slices to measure mGluR-LTD at SC to CA1 synapses. ***B***, Time course of synaptic changes induced by bath application of 100 μM DHPG during 5 min in WT ($n = 9$ slices, $N = 4$ mice) and *Synpo*^{KO} mice ($n = 9$ slices, $N = 5$ mice). Shown are representative field potentials before and after DHPG. ***C***, Quantification of average mGluR-LTD in the last 10 min of the recording. Data are mean ± SEM. *Synpo*^{KO} 87% ± 3, WT 69% ± 6, $n = 9$ slices. $p < 0.05$ (Mann–Whitney test). ***D***, Representative images of dendritic spine density in WT and Synpo^{KO} acute hippocampal slices treated with vehicle (Ctrl) or DHPG. Scale bar, 3 μm. ***E***, Quantification of total spine density and individual spine type density per micron. Total spine density: WT-Ctrl ($n = 10$), 1.05 ± 0.07, WT-DHPG ($n = 10$), 0.68 ± 0.08, Synpo^{KO}-Ctrl ($n = 9$), 1.21 ± 0.09, Synpo^{KO}-DHPG ($n = 9$), 1.25 ± 0.10. Stubby spine density: WT-Ctrl 0.16 ± 0.03, WT-DHPG 0.09 ± 0.01, Synpo^{KO}-Ctrl 0.16 ± 0.01, Synpo^{KO}-DHPG 0.17 ± 0.02. Mushroom spine density: WT-Ctrl 0.34 ± 0.05, WT-DHPG 0.17 ± 0.02, Synpo^{KO}-Ctrl 0.30 ± 0.03, Synpo^{KO}–DHPG 0.31 ± 0.03. Thin spine density: WT-Ctrl 0.70 ± 0.07, WT-DHPG 0.49 ± 0.03, Synpo^{KO}-Ctrl 0.75 ± 0.07, Synpo^{KO}-DHPG 0.77 ± 0.07. WT-Ctrl versus WT-DHPG: ***$p < 0.001$ (Mann–Whitney). ***F***, Representative images showing Synpo localization in dendritic spines in WT hippocampal acute slices treated with control or DHPG. Scale bar, 3 μm. ***G***, Quantification of Synpo^{+} spines in neurons in control (Ctrl) or DHPG-treated neurons. Spines/10 μm. Data are mean ± SEM. WT-Ctrl: 1.97 ± 0.25, WT-DHPG: 1.27 ± 0.19 (Mann–Whitney, not significant). ***H***, Percentage of Synpo^{+} spines relative to total mushroom spines in neurons treated with control or DHPG: WT-Ctrl 32.6% ± 6.0, WT-DHPG 30.3% ± 5.6 (Mann–Whitney, not significant).

Gp1 mGluR-induced synaptic depression could be compartmentalized to spines endowed with ER, whether the presence of Synpo is required for mGluR-LTD is currently unknown. To address this question, we used DHPG (*RS*-DHPG; 100 μM, 5 min) to induce mGluR-LTD at stimulated SC-CA1 synapses (Fig. 1*A*) in hippocampal slices from WT and *Synpo* KO mice (*Synpo*^{KO}), which lack the SA (Deller et al., 2003). In WT, DHPG induced rapid and enduring depression of evoked field potential (fEPSP) slope values compared with baseline, as measured 35 min after DHPG (fEPSPs to 69 ± 6% of baseline, $n = 9$; Fig. 1*B*,*C*). In contrast, in *Synpo*^{KO} mice, the capacity of DHPG to produce LTD was drastically impaired (depression of fEPSPs to 87 ± 3% of baseline, $n = 9$; Fig. 1*B*,*C*). Thus, this finding indicates that expression of Synpo and presence of the SA are required for efficient mGluR-LTD at SC-CA1 synapses.

Spines with Synpo are spared from elimination by mGluR-LTD

NMDAR-dependent LTD was shown to causes spine shrinkage and elimination (Stein and Zito, 2019), but whether mGluR-LTD is accompanied with spine elimination remains controversial. Both spine shrinkage and elimination (Ramiro-Cortés and Israely, 2013) and, conversely, absence of changes in structural plasticity and spine density (Thomazeau et al., 2021), were reported in response to Gp1 mGluR activation. To test whether deficits in mGluR-LTD in *Synpo*^{KO} mice are accompanied by changes in spine elimination or structural plasticity, we measured dendritic protrusions in WT and *Synpo*^{KO} hippocampal slices before and after induction of mGluR-LTD, taking advantage of a GFP transgene expressed in both genotypes that facilitates visualization of dendritic spines (Verbich et al., 2016). In response to DHPG, we observed a rapid, overall loss of dendritic spines in WT but not *Synpo*^{KO} mice (Fig. 1*D*,*E*) that was driven by a selective decrease in the stronger mushroom spines, whereas the density of weaker thin and stubby spines was not altered (Fig. 1*D*,*E*). The impact of mGluR-LTD on mushroom spines containing Synpo/SA is unknown. To explore this, WT hippocampal slices before or after induction of mGluR-LTD were immunolabeled with anti-Synpo to visualize mushroom spines in which Synpo is present (Synpo^{+}; Fig. 1*F*). We found that the

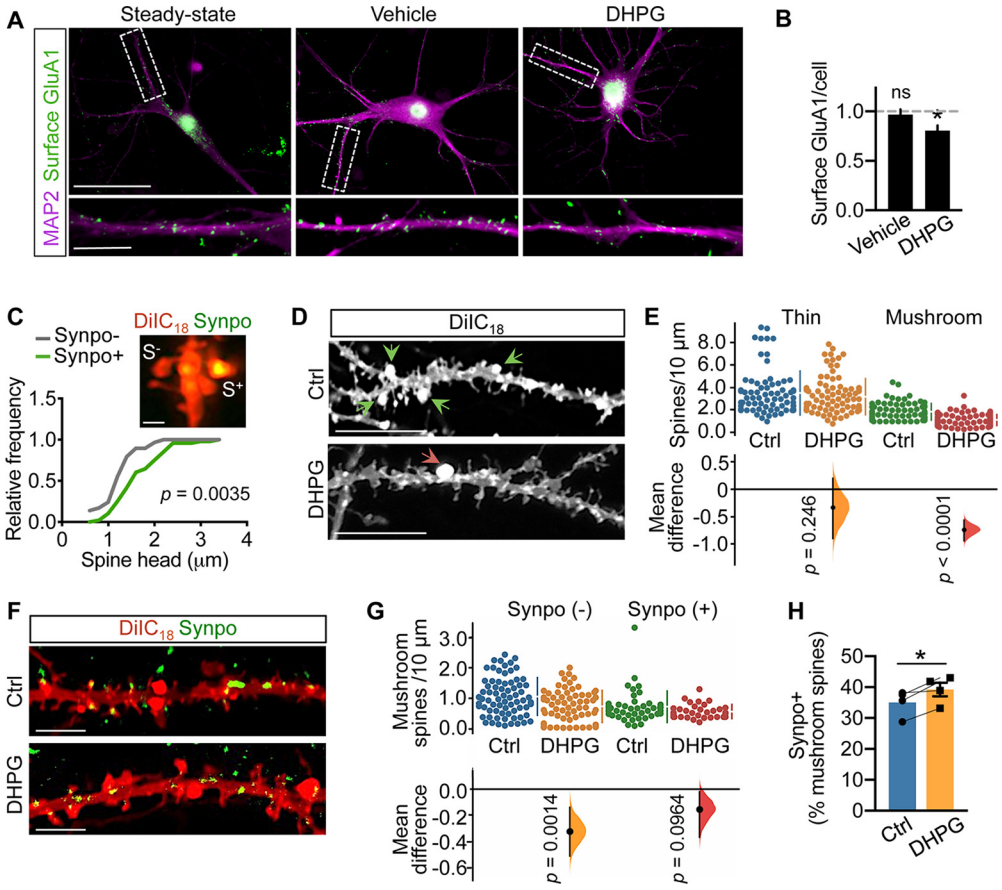

Figure 2. Mushroom spines with Synpo are spared from elimination by mGluR-LTD. ***A***, Representative images of surface GluA1 in MAP2-labeled dendrites of rat hippocampal neurons at steady state (untreated), treated with vehicle or DHPG followed by 30 min recovery. Scale bar: 50 μm; inset, 10 μm. ***B***, Quantification of surface GluA1 puncta per cell (fold steady state) from images as in ***A***. Data are mean ± SE. Steady state 1.0 ± 10.039 ($n = 13$), vehicle 0.97 ± 0.052 ($n = 13$), DHPG 0.81 ± 0.051 ($n = 11$). *$p = 0.019$ (ANOVA with Tukey's post-test). ***C***, Properties of mushroom spines with or without Synpo in primary rat hippocampal neurons. Representative image (Airyscan) of spines in neurons labeled with $DiIC_{18}$ and anti-Synpo. S^+, Spines with Synpo; S^-, spines without Synpo. Scale bar, 0.5 μm. Relative frequency distribution of spine head dimensions: $Synpo^-$ ($n = 29$), $Synpo^+$ ($n = 48$), Kolmogorov–Smirnov test. ***D***, Images of $DiIC_{18}$-labeled neurons treated with vehicle (Ctrl) or mGluR-LTD (DHPG; 30 min recovery). Arrowheads indicate mushroom spines. Scale bars, 10 μm. ***E***, Quantification of thin and mushroom spine density per 10 μm. Data are mean ± SD. Thin spines, Ctrl 3.5 ± 2.0 ($n = 74$ dendritic branches), DHPG 3.2 ± 1.6 ($n = 91$), $N = 36$ cells per group. $p = 0.246$ (two-sided permutation t test). Mushroom spines, Ctrl 1.9 ± 0.74 ($n = 78$), DHPG 1.1 ± 0.50 ($n = 109$), $N = 45$ cells, $p < 0.0001$. Gardner–Altman estimation plot: mean difference (dot, bottom) is plotted on a floating axis as a bootstrap sampling distribution. Vertical error bars indicate the 95% CI (two-sided permutation t test). ***F***, Representative images of hippocampal neurons treated with vehicle (Ctrl) or DHPG (30 min recovery) and labeled with $DiIC_{18}$ and anti-Synpo antibody. Scale bars, 4 μm. ***G***, Quantification of the density (spines/10 μm) of $Synpo^-$ and $Synpo^+$ mushroom spines in neurons treated with vehicle (Ctrl) or DHPG from images like those in ***D***. Data are mean ± SD. $Synpo^-$, Ctrl 1.1 ± 0.61 ($n = 73$), DHPG 0.74 ± 0.52 ($n = 70$); $Synpo^+$, Ctrl 0.73 ± 0.51 ($n = 45$), DHPG 0.58 ± 0.23 ($n = 34$), $N = 30$ cells per group. Gardner–Altman estimation plot (two-sided permutation t test). ***H***, Percentage of $Synpo^+$ spines relative to total mushroom spines in neurons treated with vehicle (Ctrl) or mGluR-LTD (30 min). Data are mean ± SE from $N = 4$ experiments. $p = 0.04$ (paired t test).

density and relative percentage of $Synpo^+$ spines were not significantly affected by mGluR-LTD (Fig. 1*F–H*), suggesting that mushroom spines containing Synpo remain stable, whereas those lacking Synpo are lost.

Perturbations in spine density and morphologic properties can occur in acute slices, likely linked to nonphysiological temperature (Kirov et al., 1999; Bourne et al., 2007; Trivino-Paredes et al., 2019; Eguchi et al., 2020) and lack of supporting nutrients. To survey the impact of mGluR-LTD on spine properties under physiological conditions that preserve actin dynamics (Roelandse and Matus, 2004; McKinney, 2010) and rate of protein synthesis (Cooke et al., 2019), both crucial for structural and functional plasticity (Huber et al., 2000; Cingolani and Goda, 2008), widespread chemical mGluR-LTD was produced by transient stimulation of mature primary rat hippocampal neurons with *S*-DHPG (50 μM, 15 min) followed by recovery for 30 or 120 min, corresponding to early and late times after induction when LTD is fully expressed. In concurrence with previous data (Snyder et al., 2001), chemical mGluR-LTD (mGluR-LTD hereafter) decreased the surface abundance of the GluA1 subunit of AMPARs, attesting to the effectiveness of the LTD protocol (Fig. 2*A*,*B*). Synpo is expressed in spines starting around postnatal day 12, and is most abundant in the adult brain (Czarnecki et al., 2005). Remarkably, Synpo developmental regulation is mirrored in primary neurons (Konietzny et al., 2019), where Synpo is detected at ~1 week of differentiation *in vitro* and increases over time, peaking at ~3 weeks. In primary rat hippocampal neurons, congruent with its localization in intact tissue, Synpo occupies the neck and head of mushroom spines (Fig. 2*C*), ~50% of which are of size comparable to mushroom spines lacking Synpo so that they are not distinguishable based on morphology alone (Fig. 2*C*). The impact of mGluR-LTD on the density and morphologic properties of dendritic spines was examined using sparse labeling of hippocampal neurons with the fluorescent lipophilic dye $DiIC_{18}$ and high-resolution microscopy. We found that mGluR-LTD resulted in a net decrease in the overall density of dendritic protrusions at 30 min after treatment (total protrusions/10 μm, mean ± SD, vehicle 3.7 ± 1.1,

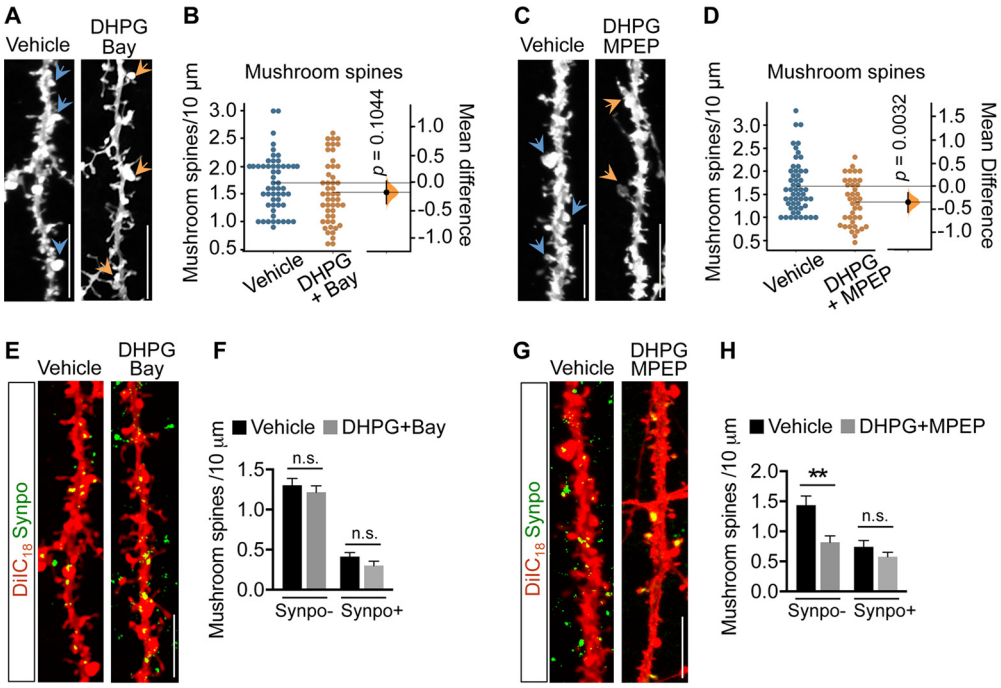

Figure 3. mGluR-LTD induces loss of Synpo-lacking mushroom spines through activation of mGluR1. ***A***, Representative images of hippocampal neurons treated with vehicle or DHPG in the presence of Bay (30 min recovery) and labeled with $DiIC_{18}$: arrowheads point to mushroom spines. Scale bars, 10 μm. ***B***, Quantification of mushroom spine density from images like those in ***A***. Data are mean ± SD. Vehicle 1.7 ± 0.50 ($n = 55$), DHPG+Bay 1.5 ± 0.57 ($n = 49$), $N = 25$ cells per group. $p = 0.1044$ (two-sided permutation t test). ***C***, Representative images of hippocampal neurons treated with vehicle or DHPG in the presence of MPEP (30 min recovery) and labeled with $DiIC_{18}$. Scale bars, 10 μm. ***D***, Quantification of mushroom spine density from images like those in ***C***. Data are mean ± SD. Vehicle 1.7 ± 0.57 ($n = 53$), DHPG+MPEP 1.3 ± 0.49 ($n = 40$) from 3 experiments. $p = 0.0032$ (two-sided permutation t test). ***E***, Representative images of hippocampal neurons treated with vehicle or DHPG in the presence of Bay (30 min recovery) and labeled with $DiIC_{18}$ and anti-Synpo. Scale bars, 10 μm. ***F***, Quantification of the density of $Synpo^-$ and $Synpo^+$ mushroom spines from images like those in ***E***. Data are mean ± SEM. $Synpo^-$ vehicle 1.3 ± 0.084 ($n = 63$), DHPG+Bay 1.2 ± 0.079 ($n = 50$), $Synpo^+$ vehicle 0.41 ± 0.049 ($n = 63$), DHPG+Bay 0.30 ± 0.054 ($n = 47$) from 3 experiments (not significant). $p > 0.05$ (unpaired t test). ***G***, Representative images of hippocampal neurons treated with vehicle or DHPG in the presence of MPEP (30 min recovery) and labeled with $DiIC_{18}$ and anti-Synpo. ***H***, Quantification of the density of $Synpo^-$ and $Synpo^+$ mushroom spines from images like those in ***G***. Data are mean ± SEM. $Synpo^-$ Vehicle 1.4 ± 0.15 ($n = 17$), DHPG+MPEP 0.82 ± 0.11 ($n = 22$), $Synpo^+$ vehicle 0.74 ± 0.11 ($n = 12$), DHPG+MPEP 0.58 ± 0.073 ($n = 21$) from 2 experiments. $^{**}p = 0.0017$ (unpaired t test).

$n = 54$ dendritic branches vs mGluR-LTD, 2.7 ± 0.76, $n = 78$ from $N = 30$ neurons per group; $p < 0.001$, Mann–Whitney test). Categorization of spines based on established morphologic criteria indicated that mGluR-LTD produced net loss of the synaptically stronger mushroom spines, whereas the density of thin spines was unaffected (Fig. 2*D*,*E*).

We next tested whether the observed net loss of mushroom spines induced by mGluR-LTD included spines containing Synpo. Visualization of endogenous Synpo by immunolabeling of neurons filled with $DiIC_{18}$ shows that, as in the hippocampus where ~10% of total spines contain Synpo/SA, in primary hippocampal neurons ~13% of all dendritic protrusions contain Synpo (mean ± SD, 13 ± 4.6%, $n = 17$), accounting for ~30% of mushroom spines (mean ± SD, 32 ± 13%, $n = 44$). Congruent with observations in hippocampal slices, we found that, despite net loss of mushroom spines lacking Synpo ($Synpo^-$), the density of Synpo-containing spines ($Synpo^+$) did not significantly differ after mGluR-LTD compared with control (Fig. 2*F*,*G*), so that the relative frequency of $Synpo^+$ versus total mushroom spines was modestly increased by mGluR-LTD (Fig. 2*H*).

Both mGluR1 and mGluR5 contribute to induction of mGluR-LTD by DHPG, but only selective inhibition of mGluR1 was shown to revert LTD and AMPAR internalization (Volk et al., 2006), suggesting distinct receptor functions. To test whether both mGluR1 and mGluR5 play a role in net loss of Synpo-lacking mushroom spines, mGluR-LTD was induced in the presence of either Bay (10 μM) or 2-methyl-6-(phenylethynyl) pyridine (MPEP; 10 μM), selective inverse agonists for mGluR1 and mGluR5, respectively. We found that whereas Bay halted mGluR-LTD-induced net loss of mushroom spines (Fig. 3*A*,*B*), MPEP had no significant effect (Fig. 3*C*,*D*). Visualization of Synpo-labeled mushroom spines in neurons stained with $DiIC_{18}$ confirmed that inhibition of mGluR1 with Bay, but not inhibition of mGluR5, prevented DHPG-induced selective loss of $Synpo^-$ mushroom spines (Fig. 3*E*–*H*). Collectively, these findings indicate that spines containing stable Synpo are a primary locus of the plasticity. mGluR-LTD induces selective loss of mushroom spines that do not contain Synpo, whereas those in which Synpo/SA is present are spared, a process that is dependent on mGluR1 activation during mGluR-LTD.

mGluR-LTD induces compartment-specific degradation of Synpo

Our findings indicate that the proportion of mature mushroom spines tagged by Synpo remains constant in response to mGluR-LTD, suggesting that overall only mushroom spines in which Synpo is absent are lost. Hence, whereas spines tagged by Synpo and SA remain stable, those "untagged" are eliminated. If so, how can Synpo "tagging" be restricted to subsets of spines? One possibility is that Synpo expression and availability for recruitment to spines could be constrained. In addition to being localized in spines, Synpo is present in dendritic shafts where it appears in discrete clusters and occasional tubule-like structures (Deller et al., 2000; Konietzny et al., 2019). Various synaptic activity patterns were previously shown to regulate Synpo expression, including LTP (Yamazaki et al., 2001) and denervation-induced

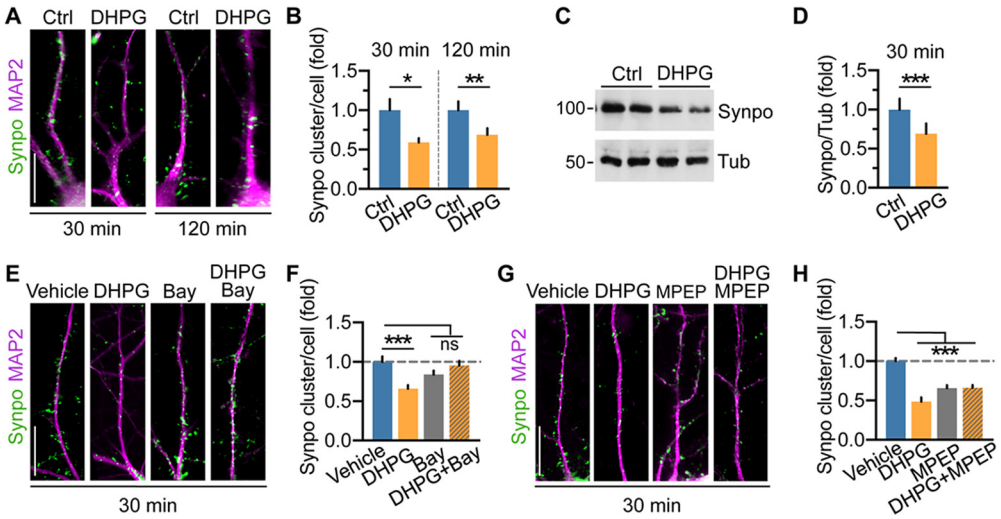

Figure 4. mGluR-LTD induces degradation of Synpo in dendritic shafts. ***A***, Representative images and quantification of immunolabeled Synpo in MAP2-positive dendrites of hippocampal neurons treated with vehicle (Ctrl) or DHPG followed by recovery for 30 or 120 min. Scale bars, 15 μm. ***B***, Quantification of dendritic Synpo clusters per cell (fold vehicle) from images as in ***A***. Data are mean ± SE. 30 min, Ctrl 1.0 ± 0.14, DHPG 0.59 ± 0.053, $n = 71$ cells per group from $N = 6$ experiments. *$p = 0.0106$ (120 min). Ctrl 1.0 ± 0.111 ($n = 44$), DHPG 0.69 ± 0.083 ($n = 45$), $N = 4$. **$p = 0.004$ (paired t test). ***C***, Representative immunoblot of cortical neurons treated with vehicle (Ctrl) or DHPG followed by 30 min recovery: tubulin (Tub), loading control. ***D***, Quantification of Synpo (fold Ctrl) from blots as in ***C***. Data are mean ± SE. Ctrl 1.0 ± 0.14, DHPG 0.69 ± 0.13, $N = 5$. ***$p = 0.0002$ (paired t test). ***E***, Representative images of Synpo in hippocampal neurons treated with vehicle, Bay, or DHPG (in the presence/absence of Bay) followed by 30 min recovery. Scale bar, 15 μm. ***F***, Quantification of Synpo clusters from images as in ***E***. Data are mean ± SE. Vehicle 1.0 ± 0.069 ($n = 17$), DHPG 0.66 ± 0.044 ($n = 28$), Bay 0.84 ± 0.049 ($n = 26$), DHPG+Bay 0.95 ± 0.058 ($n = 18$) from 2 experiments. ***$p < 0.001$. Not significant, $p > 0.1$ (one-way ANOVA with Tukey's post-test). ***G***, Representative images of Synpo in hippocampal neurons treated with vehicle, MPEP, or DHPG in the presence/absence of MPEP followed by 30 min recovery. Scale bar, 15 μm. ***H***, Quantification of Synpo clusters from images as in ***G***. Data are mean ± SE. Vehicle 1.0 ± 0.039 ($n = 29$), DHPG 0.49 ± 0.052 ($n = 16$), MPEP 0.66 ± 0.038 ($n = 32$), DHPG+MPEP 0.66 ± 0.035 ($n = 31$); from 4 experiments. ***$p < 0.001$ (one-way ANOVA with Tukey's post-test).

synaptic strengthening (Vlachos et al., 2013) that increase Synpo biosynthesis or enlargement of Synpo clusters, respectively. In contrast, homeostatic synaptic downscaling in elevated activity induces a decrease in Synpo abundance (Dörrbaum et al., 2020). Thus, we next examined the impact of mGluR-LTD on Synpo expression using immunofluorescence in primary hippocampal neurons to visualize dendritic Synpo clusters, and immunoblot in cortical neurons to monitor changes in Synpo abundance. In dendrites visualized by MAP2, mGluR-LTD reduced the density of Synpo clusters per cell within 30 min of stimulation, an effect that persisted at 120 min after DHPG (Fig. 4*A*,*B*). In line with results by immunofluorescence, the total abundance of Synpo protein was similarly reduced in cortical neurons after mGluR-LTD (Fig. 4*C*,*D*). We next tested whether both mGluR1 and mGluR5 contributed to the loss of dendritic Synpo by inducing mGluR-LTD in the presence of either Bay or MPEP, respectively. In the presence of Bay, mGluR-LTD failed to decrease Synpo clusters, whereas Bay alone had no significant effect (Fig. 4*E*,*F*). In contrast, in the presence of MPEP, mGluR-LTD effectively reduced dendritic Synpo clusters and application of MPEP alone caused a decrease in Synpo (Fig. 4*G*,*H*). Synpo turnover, the balance of its *de novo* synthesis and degradation, is dynamically regulated by activity (Dörrbaum et al., 2020). Since mGluR5 is a constitutively active receptor (Joly et al., 1995; Ango et al., 2001) that can induce *de novo* protein synthesis (Stoppel et al., 2017), we reasoned that the effect of the inverse agonist MPEP may arise from suppressing mGluR5-dependent Synpo synthesis, potentially mediated via basal mGluR5 signaling to mTOR (Richter and

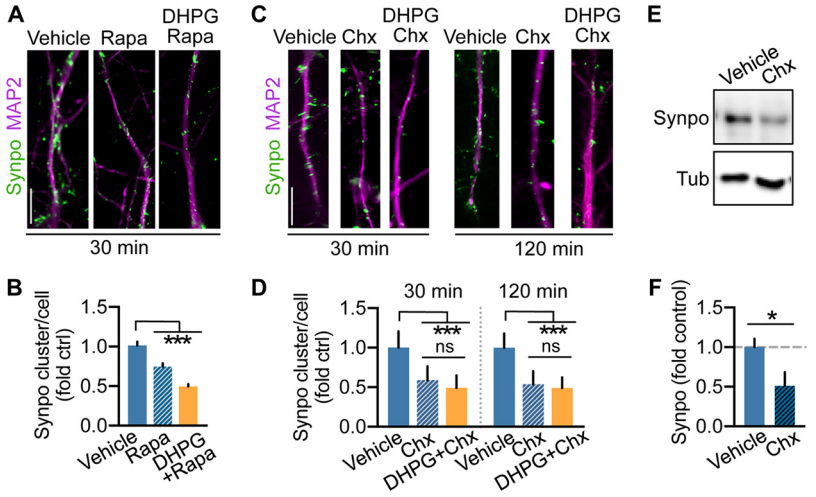

Figure 5. Basal expression of Synpo is regulated by mTOR and ongoing protein synthesis. ***A***, Representative images of immunolabeled Synpo in MAP2-positive dendrites of hippocampal neurons treated with vehicle, rapamycin (20 nM), or DHPG in the presence of rapamycin (30 min recovery). Scale bars, 10 μm. ***B***, Quantification of Synpo clusters per cell (fold control vehicle) from images as in ***A***. Data are mean ± SE. Vehicle 1.0 ± 0.048 ($n = 23$), rapamycin 0.75 ± 0.042 ($n = 40$), DHPG+rapamycin 0.50 ± 0.031 ($n = 30$), 2 experiments. ***$p < 0.001$ (one-way ANOVA with Tukey's post-test). ***C***, Representative images of dendritic Synpo in hippocampal neurons treated with vehicle or Chx (50 μM) alone for 30 and 120 min, or Chx after DHPG (15 min). Scale bar 10 μm. ***D***, Quantification of Synpo clusters (fold vehicle) from images as in ***C***. Data are mean ± SE. 30 min, vehicle 1.0 ± 0.038 ($n = 30$), Chx 0.59 ± 0.029 ($n = 35$), DHPG/Chx 0.49 ± 0.027 ($n = 34$); 120 min vehicle 1.0 ± 0.035 ($n = 26$), Chx 0.54 ± 0.027 ($n = 39$), DHPG/Chx 0.49 ± 0.025 ($n = 31$) from 3 experiments. ***$p < 0.001$ (one-way ANOVA with Tukey's post-test). ***E***, Representative immunoblot of cortical neurons treated with vehicle or Chx for 120 min. ***F***, Quantification of total Synpo from blots as in ***E***. Data are mean ± SE. Vehicle 1.0 ± 0.11 ($n = 5$), Chx 0.51 ± 0.17 ($n = 5$), 2 experiments. *$p = 0.042$ (two-tailed unpaired t test).

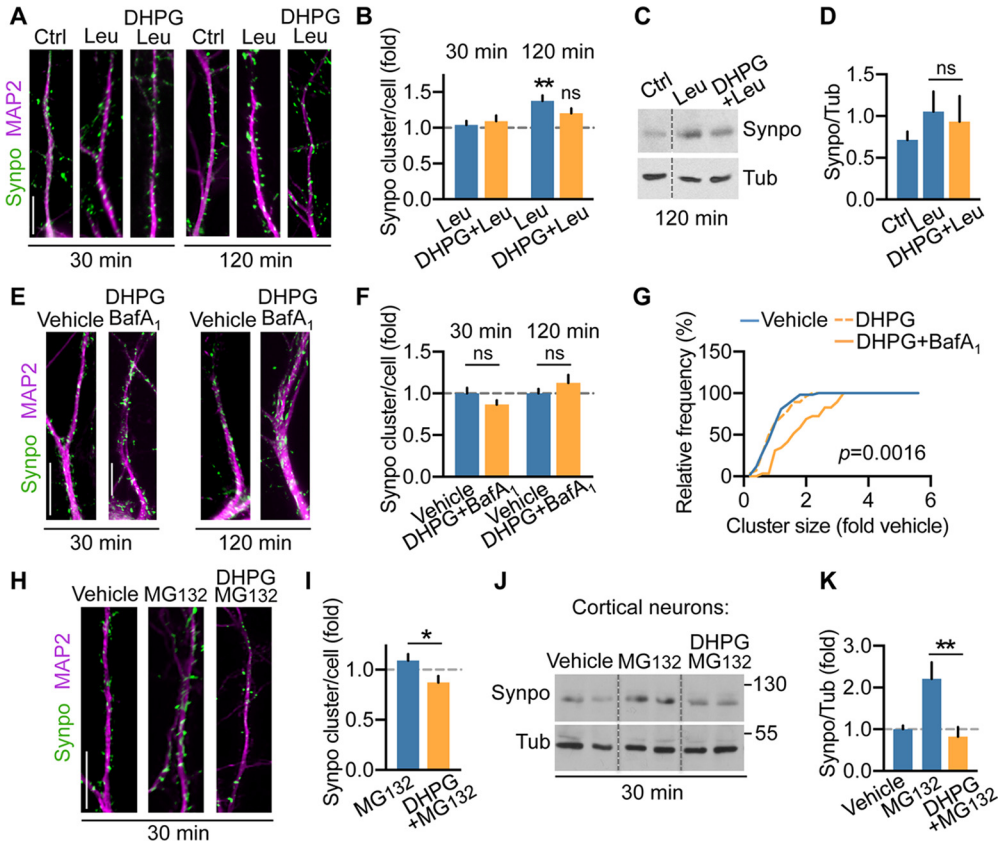

Figure 6. mGluR-LTD promotes Synpo degradation via lysosomal proteolysis. ***A***, Representative images of Synpo in hippocampal neurons treated with vehicle (Ctrl), leupeptin (Leu), DHPG in the presence/absence of leupeptin for 30 or 120 min. ***B***, Quantification of Synpo clusters from images as in ***A***. Data are mean ± SE. 30 min, Ctrl 1.0 ± 0.06 ($n = 30$), Leu 1.04 ± 0.054 ($n = 35$), DHPG+Leu 1.1 ± 0.079; 120 min, Ctrl 1.0 ± 0.076 ($n = 19$), Leu 1.4 ± 0.076 ($n = 36$), DHPG+Leu 1.2 ± 0.07 ($n = 26$), 2 experiments; (not significant) $p = 0.22$. $^{**}p = 0.004$ (ANOVA, Tukey's post-test). ***C***, Representative immunoblot of cortical neurons treated with vehicle (Ctrl), Leu, DHPG in the presence of Leu (120 min recovery); tubulin (Tub), loading control. ***D***, Quantification of blots as in ***C***. Total Synpo (fold Tub): mean ± SE, Ctrl 0.71 ± 0.05, Leu 1.1 ± 0.12, DHPG+Leu 0.93 ± 0.15, 4 independent determinations (not significant). $p = 0.640$ (two-tailed unpaired t test). ***E***, Representative images of Synpo in hippocampal neurons treated with vehicle or DHPG in the presence of $BafA_1$ for 30 or 120 min. Scale bar, 15 μm. ***F***, Quantification of Synpo clusters from images as in ***E***. Data are mean ± SE. 30 min, vehicle 1.0 ± 0.066 ($n = 24$), DHPG+$BafA_1$ 0.87 ± 0.049 ($n = 36$), 2 experiments (not significant), $p = 0.41$; 120 min, vehicle 1.0 ± 0.054, ($n = 26$), DHPG+$BafA_1$ 1.13 ± 0.095 ($n = 20$) (not significant). $p = 0.56$ (ANOVA, Tukey's post-test). ***G***, Distribution of Synpo cluster size (fold vehicle) in hippocampal neurons treated with vehicle ($n = 53$) or DHPG (30 min recovery) in the absence ($n = 28$) or presence of $BafA_1$ ($n = 29$); Kolmogorov–Smirnov test. ***H***, Representative images of Synpo in hippocampal neurons treated with vehicle, MG132, DHPG+MG132 followed by recovery in MG132 (30 min). Scale bar, 15 μm. ***I***, Quantification of Synpo clusters from images as in ***H***. Data are mean ± SE. Vehicle 1.0 ± 0.083 ($n = 20$), MG132 1.1 ± 0.064 ($n = 27$), DHPG+MG132 0.87 ± 0.064 ($n = 25$), 2 experiments. $^{*}p = 0.0196$ (two-tailed unpaired t test). ***J***, Representative blot of cortical neurons treated with vehicle, MG132, DHPG+MG132 with recovery in the presence of MG132. ***K***, Quantification of Synpo from blots as in ***J***. Data are mean ± SE. Vehicle 1.0 ± 0.088 ($n = 10$), MG132 2.2 ± 0.39 ($n = 5$), DHPG+MG132 0.82 ± 0.23 ($n = 7$), 3 experiments. $^{**}p = 0.001$ (ANOVA, Tukey's post-test).

Klann, 2009). Incubation with the mTOR inhibitor rapamycin reduced the density of dendritic Synpo clusters that was further decreased by application of DHPG in the presence of rapamycin (Fig. 5*A*,*B*) suggesting involvement of mTOR in Synpo turnover. In non-neuronal cells, inhibition of mTOR with rapamycin not only reduces protein synthesis but also promotes macroautophagy initiation (Laplante and Sabatini, 2009), although the latter effect is not observed in neurons (Maday and Holzbaur, 2016). Nevertheless, to distinguish between these possibilities, neurons were incubated with the protein synthesis inhibitor cycloheximide (Chx) either alone for 30 or 120 min or after DHPG. We found that cycloheximide rapidly and robustly reduced Synpo clusters (Fig. 5*C*,*D*) and abundance (Fig. 5*E*,*F*), with DHPG producing a modest further decrease (not statistically significant; Fig. 5*C*,*D*). Together, these results indicate that constitutive synthesis of Synpo (Dörrbaum et al., 2020) is partly mediated by mTOR activation, potentially downstream of mGluR5, which does not occlude mGluR-LTD capacity to induce degradation of dendritic Synpo via mGluR1.

mGluR-LTD promotes Synpo degradation via lysosomal proteolysis

Synpo is a natively unfolded protein (Chalovich and Schroeter, 2010), the primary structure of which includes proline-rich regions that mark unstable proteins. Natively unfolded proteins tend to form aggregates that can be cleared via autophagy through lysosomal digestion (Lamark and Johansen, 2012). To test whether lysosomal proteolysis contributes to Synpo turnover, hippocampal neurons were treated with leupeptin (Leu; 200 μM), an inhibitor of lysosomal cysteine, serine and threonine peptidases, for either 30 or 120 min. In these conditions, the density of Synpo clusters was not significantly altered after 30 min but increased over 120 min (Fig. 6*A*,*B*) concordant with a leupeptin-dependent increase in total Synpo in cortical neurons (Fig. 6*C*,*D*). Induction of mGluR-LTD in the presence of leupeptin failed to reduce the number of dendritic Synpo clusters (30 and 120 min; Fig. 6*A*,*B*) and to decrease total Synpo protein abundance (Fig. 6*C*,*D*). To confirm a role of lysosomal proteolysis in this process, we used bafilomycin A_1 ($BafA_1$; 100 nM), a V-ATPase inhibitor that prevents lysosome acidification and also

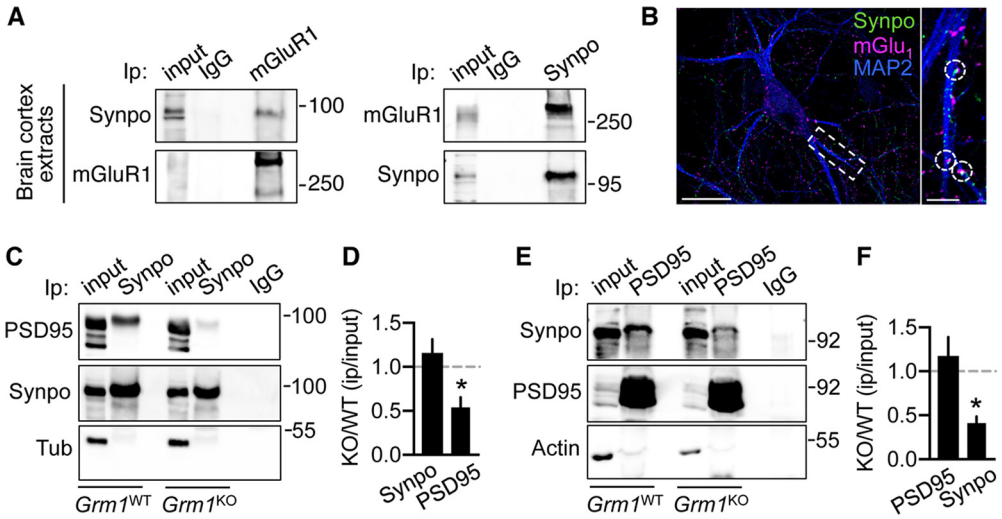

Figure 7. mGluR1 enables Synpo stabilization at excitatory spine synapses. ***A***, Synpo coprecipitates with mGluR1. Representative immunoprecipitation (Ip) with anti-mGluR1 or control IgG probed for Synpo (left) and with anti-Synpo or IgG probed for mGluR1 (right) from extracts of brain cortex of adult WT mice. ***B***, Representative images of rat hippocampal neurons labeled for mGluR1, Synpo, and MAP2. MGluR1 puncta are found in apposition to Synpo: 17 ± 5.5% of Synpo puncta in MAP2-labeled dendrites ($n = 29$ branches, $N = 13$ cells) are apposed to mGluR1. Scale bars: 50 μm; inset, 10 μm. ***C***, Coprecipitation of PSD95 with Synpo in $Grm1^{WT}$ and $Grm1^{KO}$ mice: representative blot probed for PSD95 of immunoprecipitation with anti-Synpo antibody from lysates of brain cortex of adult mice. Input, 5% of Ip lysate; tubulin (Tub), loading control. ***D***, Quantification of PSD95 coprecipitation with Synpo from blots as in ***C***. Mean ± SE, KO/WT PSD95 0.54 ± 0.12, KO/WT Synpo 1.2 ± 0.16, $N = 3$ mice per group. *$p = 0.0329$ (two-tailed unpaired t test). ***E***, Coprecipitation of Synpo with PSD95 in $Grm1^{WT}$ and $Grm1^{KO}$ mice: representative blot probed for Synpo of immunoprecipitation with anti-PSD95 or control IgG from lysates of brain cortex of adult mice. Input, ~2% of Ip lysate; actin, loading control. ***F***, Quantification of Synpo coprecipitation with PSD95 from blots as in ***E***. Mean ± SE, KO/WT Synpo 0.41 ± 0.075, KO/WT PSD95 1.2 ± 0.21, $N = 3$ mice per group. *$p = 0.0271$ (two-tailed unpaired t test).

blocks autophagosome–lysosome fusion (Mauvezin et al., 2015). In the presence of $BafA_1$, mGluR-LTD failed to decrease dendritic Synpo (Fig. 6*E*,*F*) but did produce a modest enlargement of individual Synpo clusters compared with vehicle or mGluR-LTD alone (Fig. 6*G*), suggesting accumulation of Synpo in disabled lysosomes.

Next, we tested whether the proteasome could also participate to DHPG-induced Synpo degradation since proteasome activity was shown to contribute to protein turnover during mGluR-LTD (Hou et al., 2006; Citri et al., 2009; Klein et al., 2015) and homeostatic downscaling (Dörrbaum et al., 2020). Treatment of hippocampal neurons with the proteasome inhibitor MG132 (10 μM, 30 min) produced a modest (not statistically significant) increase in the density of dendritic Synpo but did not block mGluR-LTD-induced loss of Synpo clusters (Fig. 6*H*,*I*). Similarly, incubation with MG132 increased total Synpo abundance in cortical neurons but did not prevent mGluR-LTD-induced degradation (Fig. 6*J*,*K*), suggesting that, although Synpo turnover is partly mediated by the proteasome, its degradation by mGluR-LTD is proteasome-independent. Together, these results indicate that mGluR-LTD induces rapid degradation of dendritic Synpo via the lysosomal pathway.

mGluR1 contributes to Synpo stabilization in dendritic spines

Our findings indicate that mGluR-LTD, primarily through activation of mGluR1, triggers selective degradation of Synpo present in dendritic shafts but not of Synpo targeted to spines that are spared by mGluR-LTD-dependent elimination. These observations raise the question of how Synpo could be stabilized and shielded from degradation in spines. Synpo, an actin-bundling protein, is recruited to spines through association with α-actinins (Asanuma et al., 2005; Kremerskothen et al., 2005), including α-actinin-4, which directly binds mGluR1 and is preferentially enriched in large spine heads (Kalinowska et al., 2015). We reasoned that Synpo might be physically tethered to mGluR1 via a multivalent complex formed with actinins contributing to its stabilization in spines. Coimmunoprecipitation assays show that anti-mGluR1 pulls down Synpo from brain cortex extracts of adult WT mice and anti-Synpo retrieves mGluR1 (Fig. 7*A*), whereas by immunolabeling mGluR1 can be detected in close apposition with Synpo in hippocampal neurons (Fig. 7*B*).

Synpo is retrieved in the postsynaptic density (PSD) fraction of excitatory synapses (Bayés et al., 2012) and was shown to be linked to core scaffold proteins associated with the PSD (Li et al., 2017). To test whether mGluR1 contributes to Synpo stabilization at excitatory spine synapses, we used mGluR1 KO mice ($Grm1^{KO}$) to probe Synpo association with the PSD in absence of the receptor. Immunoprecipitation of Synpo from brain cortex of adult WT littermates ($Grm1^{WT}$) effectively retrieved PSD95, a core component of the PSD (Fig. 7*C*): in contrast, pull-down of PSD95 with Synpo was decreased in $Grm1^{KO}$ mice (Fig. 7*C*,*D*) in the absence of significant alterations in the relative abundance of the proteins (mean ± SE, $Grm1^{WT}$ Synpo 2.2 ± 0.25, $Grm1^{KO}$ 1.7 ± 0.21 $N = 3$ mice per group, $p = 0.1897$; $Grm1^{WT}$ PSD95 2.5 ± 0.64, $Grm1^{KO}$ 2.7 ± 0.82 $N = 3$, $p = 0.8641$, two-tailed unpaired t test). Similarly, the efficiency of Synpo retrieval by immunoprecipitation with anti-PSD95 was reduced in cortical tissue from $Grm1^{KO}$ mice (Fig. 7*E*,*F*), suggesting defects in the recruitment or retention of Synpo to spine synapses.

To examine whether impaired association of Synpo with the PSD may be linked to spine abnormalities in $Grm1^{KO}$ mice, we used $DiIC_{18}$ labeling to visualize dendritic spines in brain cortex tissue sections from juvenile (~1.5-month old) and adult (7-12-month old) $Gmr1^{KO}$ and $Grm1^{WT}$ littermates. We found that, in $Grm1^{KO}$ mice, the density of large mushroom spines was significantly reduced compared with WT littermates (Fig. 8*A*,*B*): moreover, the heads of remaining mushroom spines in $Grm1^{KO}$ mice were significantly smaller compared with $Grm1^{WT}$ littermates (Fig. 8*A*,*C*). We next tested for the presence of Synpo in the mushroom spines of adult $Gmr1^{KO}$ mice by immunolabeling

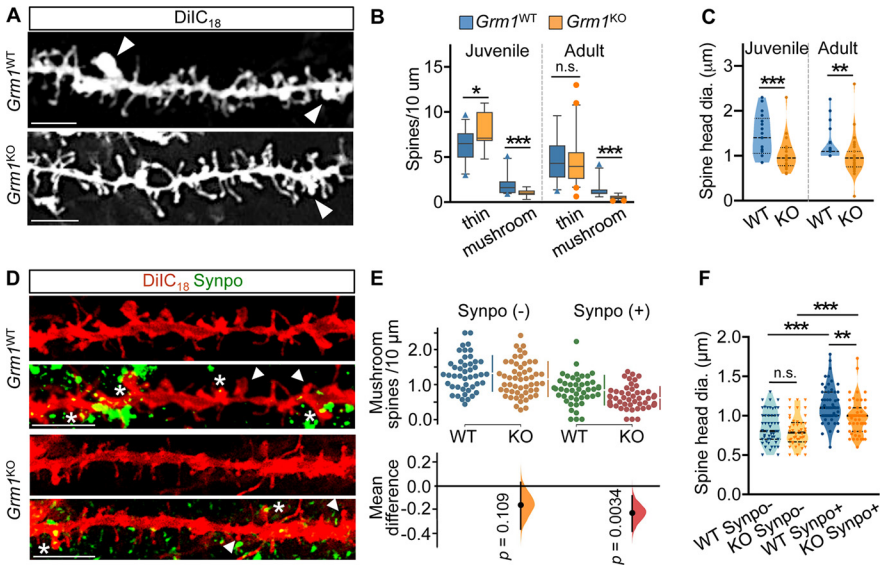

Figure 8. Reduced density and enlargement of mushroom spines with stable Synpo in mice lacking mGluR1. ***A***, Representative images of $DiIC_{18}$-labeled dendritic branches in the brain cortex of adult *Grm1*^{WT} and *Grm1*^{KO} mice: arrowheads point to mushroom spines. Scale bars, 10 μm. ***B***, Quantification of spine density per 10 μm in the cortex of *Grm1*^{WT} and *Grm1*^{KO} mice from images as in ***A***. Juvenile (~1.5 months old), mean ± SD thin spines WT 6.8 ± 1.7 ($n = 32$ dendritic branches), KO 7.8 ± 1.9 ($n = 25$). *$p = 0.025$. Mushroom spines WT 1.9 ± 0.98 ($n = 34$), KO 1.10 ± 0.39 ($n = 19$), $N = 2$ mice per group. ***$p < 0.001$. Adult mice (~7-12 months old), mean ± SD thin spines WT 4.7 ± 2.2 ($n = 36$), KO 4.4 ± 2.5 ($n = 46$) (not significant) $p = 0.29$; mushroom spines WT 1.4 ± 0.87 ($n = 31$), KO 0.54 ± 0.25 ($n = 39$), WT $N = 5$, KO $N = 4$ mice. ***$p < 0.001$, Mann–Whitney test. ***C***, Quantification of mushroom spine head dimensions (diameter) in *Grm1*^{WT} (WT) and *Grm1*^{KO} (KO) mice. Juvenile, mean ± SD, WT 1.5 ± 1.7 μm ($n = 21$), KO 1.0 ± 0.36 μm ($n = 25$). ***$p = 0.001$. Adult, mean ± SD, WT 1.2 ± 0.38 ($n = 20$), KO 1.0 ± 0.40 ($n = 40$). **$p = 0.003$, Mann–Whitney test. ***D***, Representative images of dendritic branches labeled with $DiIC_{18}$ and anti-Synpo in the brain cortex of adult *Grm1*^{WT} and *Grm1*^{KO} mice. Arrowheads point to Synpo$^-$ mushroom spines. Asterisks indicate Synpo$^+$ mushroom spines. Scale bar, 5 μm. ***E***, Quantification of the density per 10 μm of Synpo$^-$ and Synpo$^+$ mushroom spines in the cortex of adult *Grm1*^{WT} (WT) and *Grm1*^{KO} (KO) mice from images as in ***D***. Data are mean ± SD. Synpo$^-$ spines WT 1.3 ± 0.51 ($n = 46$ dendritic branches), KO 1.2 ± 0.5 ($n = 53$); Synpo$^+$ spines WT 0.85 ± 0.42, KO 0.62 ± 0.32 from 3 mice per group. Gardner–Altman estimation plot: mean difference (dot, bottom) is plotted on a floating axis as a bootstrap sampling distribution. Vertical error bars indicate the 95% CI (two-sided permutation *t* test). ***F***, Quantification of head dimensions (diameter) of Synpo$^-$ and Synpo$^+$ mushroom spines in *Grm1*^{WT} (WT) and *Grm1*^{KO} (KO) adult mice. Data are mean ± SD. Synpo$^-$ WT 0.85 ± 0.21 μm ($n = 50$), KO 0.8 ± 0.19 μm ($n = 44$); Synpo$^+$ WT 1.1 ± 0.23 μm ($n = 54$), KO 0.98 ± 0.23 μm ($n = 49$) from 3 mice per group. **$p = 0.002$; ***$p < 0.001$; one-way ANOVA with Tukey's post-test.

Synpo in combination with $DiIC_{18}$ staining (Fig. 8*D*). Interestingly, we found that, whereas the density of mushroom spines lacking Synpo (Synpo$^-$) was not significantly different between genotypes, the density of Synpo-containing spines (Synpo$^+$) was reduced in the mutant compared with WT (Fig. 8*D*,*E*). Analysis of mushroom spine morphology further revealed that, whereas the head size of Synpo$^-$ spines was comparable between genotypes, the heads of Synpo$^+$ spines were significantly smaller in *Grm1*^{KO} mice (Fig. 8*F*). Collectively, our findings indicate that, when activated during mGluR-LTD, mGluR1 promotes Synpo degradation in dendrites, whereas it locally supports Synpo stabilization in spines, possibly through formation of a multivalent protein assembly.

Discussion

Here we report that mGluR-LTD at hippocampal CA3-CA1 synapses is compromised in mice lacking Synpo and is accompanied by loss of the stronger mushroom spines in WT, but not Synpo^{KO} mice. Notably, mGluR-LTD drives selective elimination of mushroom spines in which Synpo is absent, and that therefore lack an SA, whereas spines containing Synpo remain stable. Overall, our results provide evidence that functional and structural plasticity induced by mGluR-LTD is dependent on stable Synpo spines. It has long been established that NMDAR-dependent LTD is associated with spine shrinkage/elimination (Stein and Zito, 2019), but whether mGluR-LTD induces spine structural plasticity has remained unclear. Earlier work revealed that inhibition of Gp1 mGluRs limited the shrinkage of large spines induced by low-frequency glutamate uncaging (Oh et al., 2013) and that chemical mGluR-LTD produces spine shrinkage and elimination in the CA1 region (Ramiro-Cortés and Israely, 2013). However, recent studies reported the contrasting observation of mGluR-LTD-induced synaptic weakening without accompanying changes in spine structural properties (Thomazeau et al., 2021). Although the reasons for the discrepancy remain unexplained, our findings reveal a previously unknown complex property of mGluR-LTD in promoting the elimination of selected spines that are distinguished by their molecular composition, an event that is not captured by examination of spine morphology and/or dimensions alone as in previous studies.

We show that Synpo association with stable spines is conserved *in vitro* in naive mature hippocampal neurons without prior history of activity or integrations in neural circuits. Here, the frequency of Synpo-containing spines is similar to that reported *in vivo* (Verbich et al., 2016) and, as in the intact circuitry of the hippocampal slice preparation, Synpo$^+$ mushroom spines remain stable on induction of mGluR-LTD, whereas those lacking Synpo are lost. These observations are in line with findings that the diversity of excitatory synapses of varying strength reported *in vivo* is recapitulated in neurons *in vitro*, implicating cell-intrinsic mechanisms in the generation of spine heterogeneity (Hazan and Ziv, 2020) and activity-dependent modifications. The presence of Synpo is emerging as a critical determinant of spine properties and plasticity in response to activity. Large mushroom spines containing sER, and presumably Synpo, possess higher synaptic strength (Holbro et al., 2009) and undergo slower basal turnover compared with mushroom spines in which Synpo is absent (Yap et al., 2020). Thus, mGluR-LTD may refine synaptic circuits by inducing selective elimination of weaker and unstable spines while preserving strong and stable Synpo$^+$ spines that harbor the SA. How the presence of Synpo leads to spine stabilization is unknown, but a potential mechanism may involve modification of actin cytoskeleton dynamics. Congruent with its association with the SA, Synpo is present at the base of the head and in the neck of mushroom spines, regions in which F-actin is less dynamic (Honkura et al., 2008) and concentrated between the lamellae of the SA (Capani et al., 2001). By enhancing α-actinin-dependent F-actin bundling (Asanuma et al., 2005; Kremerskothen et al., 2005), Synpo may locally depress actin cytoskeleton dynamics that are required for spine remodeling.

We find that mGluR1, engaged during mGluR-LTD, plays a complex role in the plasticity as its activation is required for

elimination of Synpo-lacking mushroom spines while the receptor contributes to the physical tethering of Synpo in spines and its concomitant removal from dendritic shafts. mGluR1 appears critical for the recruitment/stabilization of Synpo at excitatory synapses as suggested by the reduced association of Synpo with the PSD in mice lacking mGluR1. We propose that mGluR1 contributes to tethering Synpo at spine synapses via integration in a multivalent macromolecular complex formed through their respective interaction with α-actinin, which directly binds both Synpo (Asanuma et al., 2005) and mGluR1 (Kalinowska et al., 2015), is enriched in large mushroom spines, and associates with the PSD (Matt et al., 2018). Consistent with this possibility, we provide the first report of profound spine dysmorphogenesis in *Grm1*^{KO} mice. In mutant mice, mushroom spines containing Synpo are significantly less frequent and display smaller heads compared with WT littermates. Conceptually, the impact of mGluR1 on the spine "microcircuitry" is reminiscent of what observed in circuits in the cerebellum at CF-PC synapses (Hashimoto and Kano, 2013) and adult dLGN (Narushima et al., 2016) in which mGluR1 promotes stabilization of strong synaptic connections and elimination of weaker inputs.

Synpo expression is modified by activity patterns that produce plasticity, including LTP and homeostatic synaptic scaling. In hippocampal neurons in resting conditions, the turnover of Synpo is dependent on basal *de novo* synthesis and degradation via the proteasome (Dörrbaum et al., 2020). We find that basal synthesis of Synpo is dependent on mTOR activity, potentially driven by constitutive mGluR5 signaling (Joly et al., 1995; Ango et al., 2001) and further show that mGluR-LTD, via activation of mGluR1, triggers selective degradation of Synpo present in dendritic shafts. A hypothesis under consideration is that mGluR-LTD specifically targets newly synthesized Synpo, as suggested by the decrease in the pool of Synpo targeted for degradation in the presence of a protein synthesis inhibitor. Notably, mGluR-LTD appears to locally and rapidly shunt Synpo degradation to lysosomal digestion. Mechanistically, we find that Synpo degradation is not blocked by mTOR inhibition, suggesting that it is not mediated via nonselective macroautophagy (Maday and Holzbaur, 2016). Our results, however, indicate accumulation of Synpo in disabled acidic compartment(s): a potential pathway that could handle local Synpo degradation in response to mGluR-LTD, is chaperone-assisted selective autophagy that may involve Synpo interaction with specific chaperones (BAG proteins) (Ulbricht et al., 2015; Ji et al., 2019), a hypothesis that could be addressed by future studies. Nevertheless, degradation of dendritic Synpo may deplete a protein "reservoir" otherwise available for recruitment to spines. sER tubules invade and retract from spines (Wagner et al., 2011; Perez-Alvarez et al., 2020); and although untested, dendritic Synpo associated with sER could be co-recruited to spines. A potential scenario is that, by reducing dendritic Synpo availability, mGluR-LTD may exert the dual function of eliminating unstable, weaker spines and concomitantly limit spurious spine strengthening through *de novo* recruitment of Synpo.

In *Synpo*^{KO} mice, basal neurotransmission is unaffected (Deller et al., 2003) and NMDAR-dependent LTD was shown to proceed normally (Zhang et al., 2013) in contrast to mGluR-LTD that we find to be severely compromised. Thus, the reliance on stable Synpo spines appears to be a distinguishing feature of mGluR-LTD. A well-established mechanistic aspect of mGluR-LTD is that, unlike NMDAR-dependent LTD, it requires rapid protein synthesis (Huber et al., 2000). We speculate that stable Synpo spines containing the SA may provide a locus for the plasticity potentially by enabling local protein synthesis. Indeed, polyribosomes are present in proximity to the SA (Spacek and Harris, 1997; Ostroff et al., 2010), which was proposed to function as satellite secretory station based on the presence of proteins of the secretory pathway within the SA (Pierce et al., 2001). In line with this reasoning, spines of *Synpo*^{KO} mice do not undergo structural expansion during potentiation (Vlachos et al., 2009; Korkotian et al., 2014), which requires protein synthesis (Yang et al., 2008), and LTP (Deller et al., 2003; Jedlicka et al., 2009; Zhang et al., 2013) and homeostatic potentiation (Vlachos et al., 2013) are impaired in *Synpo*^{KO} mice.

In conclusion, our results identify spines with Synpo/SA as the locus of mGluR-LTD and underscore the importance of the molecular anatomy of spines in synaptic plasticity.

References

Ango F, Prézeau L, Muller T, Tu JC, Xiao B, Worley PF, Pin JP, Bockaert J, Fagni L (2001) Agonist-independent activation of metabotropic glutamate receptors by the intracellular protein Homer. Nature 411:962–965.

Asanuma K, Kim K, Oh J, Giardino L, Chabanis S, Faul C, Reiser J, Mundel P (2005) Synaptopodin regulates the actin-bundling activity of alpha-actinin in an isoform-specific manner. J Clin Invest 115:1188–1198.

Bayés A, Collins MO, Croning MD, van de Lagemaat LN, Choudhary JS, Grant SG (2012) Comparative study of human and mouse postsynaptic proteomes finds high compositional conservation and abundance differences for key synaptic proteins. PLoS One 7:e46683.

Berry KP, Nedivi E (2017) Spine dynamics: are they all the same? Neuron 96:43–55.

Bourne JN, Kirov SA, Sorra KE, Harris KM (2007) Warmer preparation of hippocampal slices prevents synapse proliferation that might obscure LTP-related structural plasticity. Neuropharmacology 52:55–59.

Capani F, Martone ME, Deerinck TJ, Ellisman MH (2001) Selective localization of high concentrations of F-actin in subpopulations of dendritic spines in rat central nervous system: a three-dimensional electron microscopic study. J Comp Neurol 435:156–170.

Chalovich JM, Schroeter MM (2010) Synaptopodin family of natively unfolded, actin binding proteins: physical properties and potential biological functions. Biophys Rev 2:181–189.

Cheng C, Trzcinski O, Doering LC (2014) Fluorescent labeling of dendritic spines in cell cultures with the carbocyanine dye 'DiI.' Front Neuroanat 8:30.

Cingolani LA, Goda Y (2008) Actin in action: the interplay between the actin cytoskeleton and synaptic efficacy. Nat Rev Neurosci 9:344–356.

Citri A, Soler-Llavina G, Bhattacharyya S, Malenka RC (2009) N-methyl-D-aspartate receptor- and metabotropic glutamate receptor-dependent long-term depression are differentially regulated by the ubiquitin-proteasome system. Eur J Neurosci 30:1443–1450.

Cooke SK, Russin J, Moulton K, Nadel J, Loutaev I, Gu Q, Li Z, Smith CB (2019) Effects of the presence and absence of amino acids on translation, signaling, and long-term depression in hippocampal slices from Fmr1 knockout mice. J Neurochem 151:764–776.

Czarnecki K, Haas CA, Bas Orth C, Deller T, Frotscher M (2005) Postnatal development of synaptopodin expression in the rodent hippocampus. J Comp Neurol 490:133–144.

Deller T, Mundel P, Frotscher M (2000) Potential role of synaptopodin in spine motility by coupling actin to the spine apparatus. Hippocampus 10:569–581.

Deller T, Korte M, Chabanis S, Drakew A, Schwegler H, Stefani GG, Zuniga A, Schwarz K, Bonhoeffer T, Zeller R, Frotscher M, Mundel P (2003) Synaptopodin-deficient mice lack a spine apparatus and show deficits in synaptic plasticity. Proc Natl Acad Sci USA 100:10494–10499.

Dörrbaum AR, Alvarez-Castelao B, Nassim-Assir B, Langer JD, Schuman EM (2020) Proteome dynamics during homeostatic scaling in cultured neurons. eLife 9:e52939.

Eguchi K, Velicky P, Hollergschwandtner E, Itakura M, Fukazawa Y, Danzl JG, Shigemoto R (2020) Advantages of acute brain slices prepared at physiological temperature in the characterization of synaptic functions. Front Cell Neurosci 14:63.

Fifková E, Markham JA, Delay RJ (1983) Calcium in the spine apparatus of dendritic spines in the dentate molecular layer. Brain Res 266:163–168.
Harris KM (2020) Structural LTP: from synaptogenesis to regulated synapse enlargement and clustering. Curr Opin Neurobiol 63:189–197.
Harris KM, Jensen FE, Tsao B (1992) Three-dimensional structure of dendritic spines and synapses in rat hippocampus (CA1) at postnatal day 15 and adult ages: implications for the maturation of synaptic physiology and long-term potentiation. J Neurosci 12:2685–2705.
Hashimoto K, Kano M (2013) Synapse elimination in the developing cerebellum. Cell Mol Life Sci 70:4667–4680.
Hazan L, Ziv NE (2020) Activity dependent and independent determinants of synaptic size diversity. J Neurosci 40:2828–2848.
Ho J, Tumkaya T, Aryal S, Choi H, Claridge-Chang A (2019) Moving beyond P values: data analysis with estimation graphics. Nat Methods 16:565–566.
Holbro N, Grunditz A, Oertner TG (2009) Differential distribution of endoplasmic reticulum controls metabotropic signaling and plasticity at hippocampal synapses. Proc Natl Acad Sci USA 106:15055–15060.
Honkura N, Matsuzaki M, Noguchi J, Ellis-Davies GC, Kasai H (2008) The subspine organization of actin fibers regulates the structure and plasticity of dendritic spines. Neuron 57:719–729.
Hou L, Antion MD, Hu D, Spencer CM, Paylor R, Klann E (2006) Dynamic translational and proteasomal regulation of fragile X mental retardation protein controls mGluR-dependent long-term depression. Neuron 51:441–454.
Huber KM, Kayser MS, Bear MF (2000) Role for rapid dendritic protein synthesis in hippocampal mGluR-dependent long-term depression. Science 288:1254–1257.
Huber KM, Gallagher SM, Warren ST, Bear MF (2002) Altered synaptic plasticity in a mouse model of fragile X mental retardation. Proc Natl Acad Sci USA 99:7746–7750.
Jedlicka P, Schwarzacher SW, Winkels R, Kienzler F, Frotscher M, Bramham CR, Schultz C, Bas Orth C, Deller T (2009) Impairment of in vivo theta-burst long-term potentiation and network excitability in the dentate gyrus of synaptopodin-deficient mice lacking the spine apparatus and the cisternal organelle. Hippocampus 19:130–140.
Ji C, Tang M, Zeidler C, Höhfeld J, Johnson GV (2019) BAG3 and SYNPO (synaptopodin) facilitate phospho-MAPT/Tau degradation via autophagy in neuronal processes. Autophagy 15:1199–1213.
Joly C, Gomeza J, Brabet I, Curry K, Bockaert J, Pin JP (1995) Molecular, functional, and pharmacological characterization of the metabotropic glutamate receptor type 5 splice variants: comparison with mGluR1. J Neurosci 15:3970–3981.
Kalinowska M, Chávez AE, Lutzu S, Castillo PE, Bukauskas FF, Francesconi A (2015) Actinin-4 governs dendritic spine dynamics and promotes their remodeling by metabotropic glutamate receptors. J Biol Chem 290:15909–15920.
Kirov SA, Sorra KE, Harris KM (1999) Slices have more synapses than perfusion-fixed hippocampus from both young and mature rats. J Neurosci 19:2876–2886.
Klein ME, Castillo PE, Jordan BA (2015) Coordination between translation and degradation regulates inducibility of mGluR-LTD. Cell Rep 10:1459–1466.
Konietzny A, González-Gallego J, Bär J, Perez-Alvarez A, Drakew A, Demmers JA, Dekkers DH, Hammer JA 3rd, Frotscher M, Oertner TG, Wagner W, Kneussel M, Mikhaylova M (2019) Myosin V regulates synaptopodin clustering and localization in the dendrites of hippocampal neurons. J Cell Sci 132:jcs230177.
Korkotian E, Frotscher M, Segal M (2014) Synaptopodin regulates spine plasticity: mediation by calcium stores. J Neurosci 34:11641–11651.
Kremerskothen J, Plaas C, Kindler S, Frotscher M, Barnekow A (2005) Synaptopodin, a molecule involved in the formation of the dendritic spine apparatus, is a dual actin/alpha-actinin binding protein. J Neurochem 92:597–606.
Lamark T, Johansen T (2012) Aggrephagy: selective disposal of protein aggregates by macroautophagy. Int J Cell Biol 2012:736905.
Laplante M, Sabatini DM (2009) mTOR signaling at a glance. J Cell Sci 122:3589–3594.
Li J, Zhang W, Yang H, Howrigan DP, Wilkinson B, Souaiaia T, Evgrafov OV, Genovese G, Clementel VA, Tudor JC, Abel T, Knowles JA, Neale BM, Wang K, Sun F, Coba MP (2017) Spatiotemporal profile of postsynaptic interactomes integrates components of complex brain disorders. Nat Neurosci 20:1150–1161.
Lüscher C, Huber KM (2010) Group 1 mGluR-dependent synaptic long-term depression: mechanisms and implications for circuitry and disease. Neuron 65:445–459.
Maday S, Holzbaur EL (2016) Compartment-specific regulation of autophagy in primary neurons. J Neurosci 36:5933–5945.
Matt L, Kim K, Hergarden AC, Patriarchi T, Malik ZA, Park DK, Chowdhury D, Buonarati OR, Henderson PB, Gökçek Saraç Ç, Zhang Y, Mohapatra D, Horne MC, Ames JB, Hell JW (2018) α-Actinin anchors PSD-95 at postsynaptic sites. Neuron 97:1094–1109.e1099.
Mauvezin C, Nagy P, Juhász G, Neufeld TP (2015) Autophagosome-lysosome fusion is independent of V-ATPase-mediated acidification. Nat Commun 6:7007.
McKinney RA (2010) Excitatory amino acid involvement in dendritic spine formation, maintenance and remodelling. J Physiol 588:107–116.
Mende M, Fletcher EV, Belluardo JL, Pierce JP, Bommareddy PK, Weinrich JA, Kabir ZD, Schierberl KC, Pagiazitis JG, Mendelsohn AI, Francesconi A, Edwards RH, Milner TA, Rajadhyaksha AM, van Roessel PJ, Mentis GZ, Kaltschmidt JA (2016) Sensory-derived glutamate regulates presynaptic inhibitory terminals in mouse spinal cord. Neuron 90:1189–1202.
Narushima M, Uchigashima M, Yagasaki Y, Harada T, Nagumo Y, Uesaka N, Hashimoto K, Aiba A, Watanabe M, Miyata M, Kano M (2016) The metabotropic glutamate receptor subtype 1 mediates experience-dependent maintenance of mature synaptic connectivity in the visual thalamus. Neuron 91:1097–1109.
Oh WC, Hill TC, Zito K (2013) Synapse-specific and size-dependent mechanisms of spine structural plasticity accompanying synaptic weakening. Proc Natl Acad Sci USA 110:E305–E312.
Oh WC, Parajuli LK, Zito K (2015) Heterosynaptic structural plasticity on local dendritic segments of hippocampal CA1 neurons. Cell Rep 10:162–169.
Ostroff LE, Cain CK, Bedont J, Monfils MH, Ledoux JE (2010) Fear and safety learning differentially affect synapse size and dendritic translation in the lateral amygdala. Proc Natl Acad Sci USA 107:9418–9423.
Perez-Alvarez A, Yin S, Schulze C, Hammer JA, Wagner W, Oertner TG (2020) Endoplasmic reticulum visits highly active spines and prevents runaway potentiation of synapses. Nat Commun 11:5083.
Pierce JP, Mayer T, McCarthy JB (2001) Evidence for a satellite secretory pathway in neuronal dendritic spines. Curr Biol 11:351–355.
Ramiro-Cortés Y, Israely I (2013) Long lasting protein synthesis- and activity-dependent spine shrinkage and elimination after synaptic depression. PLoS One 8:e71155.
Richter JD, Klann E (2009) Making synaptic plasticity and memory last: mechanisms of translational regulation. Genes Dev 23:1–11.
Roelandse M, Matus A (2004) Hypothermia-associated loss of dendritic spines. J Neurosci 24:7843–7847.
Sahin M, Sur M (2015) Genes, circuits, and precision therapies for autism and related neurodevelopmental disorders. Science 350:10.1126/science.aab3897.
Schindelin J, Arganda-Carreras I, Frise E, Kaynig V, Longair M, Pietzsch T, Preibisch S, Rueden C, Saalfeld S, Schmid B, Tinevez JY, White DJ, Hartenstein V, Eliceiri K, Tomancak P, Cardona A (2012) Fiji: an open-source platform for biological-image analysis. Nat Methods 9:676–682.
Snyder EM, Philpot BD, Huber KM, Dong X, Fallon JR, Bear MF (2001) Internalization of ionotropic glutamate receptors in response to mGluR activation. Nat Neurosci 4:1079–1085.
Spacek J (1985) Three-dimensional analysis of dendritic spines: II. Spine apparatus and other cytoplasmic components. Anat Embryol (Berl) 171:235–243.
Spacek J, Harris KM (1997) Three-dimensional organization of smooth endoplasmic reticulum in hippocampal CA1 dendrites and dendritic spines of the immature and mature rat. J Neurosci 17:190–203.
Stein IS, Zito K (2019) Dendritic spine elimination: molecular mechanisms and implications. Neuroscientist 25:27–47.
Stoppel LJ, Auerbach BD, Senter RK, Preza AR, Lefkowitz RJ, Bear MF (2017) β-Arrestin2 couples metabotropic glutamate receptor 5 to neuronal protein synthesis and is a potential target to treat fragile X. Cell Rep 18:2807–2814.

Thomazeau A, Bosch M, Essayan-Perez S, Barnes SA, De Jesus-Cortes H, Bear MF (2021) Dissociation of functional and structural plasticity of dendritic spines during NMDAR and mGluR-dependent long-term synaptic depression in wild-type and fragile X model mice. Mol Psychiatry 26:4652–4669.

Trivino-Paredes JS, Nahirney PC, Pinar C, Grandes P, Christie BR (2019) Acute slice preparation for electrophysiology increases spine numbers equivalently in the male and female juvenile hippocampus: a DiI labeling study. J Neurophysiol 122:958–969.

Ulbricht A, Gehlert S, Leciejewski B, Schiffer T, Bloch W, Höhfeld J (2015) Induction and adaptation of chaperone-assisted selective autophagy CASA in response to resistance exercise in human skeletal muscle. Autophagy 11:538–546.

Verbich D, Becker D, Vlachos A, Mundel P, Deller T, McKinney RA (2016) Rewiring neuronal microcircuits of the brain via spine head protrusions: a role for synaptopodin and intracellular calcium stores. Acta Neuropathol Commun 4:38.

Vlachos A, Ikenberg B, Lenz M, Becker D, Reifenberg K, Bas-Orth C, Deller T (2013) Synaptopodin regulates denervation-induced homeostatic synaptic plasticity. Proc Natl Acad Sci USA 110:8242–8247.

Vlachos A, Korkotian E, Schonfeld E, Copanaki E, Deller T, Segal M (2009) Synaptopodin regulates plasticity of dendritic spines in hippocampal neurons. J Neurosci 29:1017–1033.

Volk LJ, Daly CA, Huber KM (2006) Differential roles for group 1 mGluR subtypes in induction and expression of chemically induced hippocampal long-term depression. J Neurophysiol 95:2427–2438.

Wagner W, Brenowitz SD, Hammer JA 3rd (2011) Myosin-Va transports the endoplasmic reticulum into the dendritic spines of Purkinje neurons. Nat Cell Biol 13:40–48.

Wang XB, Yang Y, Zhou Q (2007) Independent expression of synaptic and morphological plasticity associated with long-term depression. J Neurosci 27:12419–12429.

Wiegert JS, Oertner TG (2013) Long-term depression triggers the selective elimination of weakly integrated synapses. Proc Natl Acad Sci USA 110: E4510–E4519.

Yamazaki M, Matsuo R, Fukazawa Y, Ozawa F, Inokuchi K (2001) Regulated expression of an actin-associated protein, synaptopodin, during long-term potentiation. J Neurochem 79:192–199.

Yang Y, Wang XB, Frerking M, Zhou Q (2008) Spine expansion and stabilization associated with long-term potentiation. J Neurosci 28:5740–5751.

Yap K, Drakew A, Smilovic D, Rietsche M, Paul MH, Vuksic M, Del Turco D, Deller T (2020) The actin-modulating protein synaptopodin mediates long-term survival of dendritic spines. eLife 9: e62944.

Zagrebelsky M, Holz A, Dechant G, Barde YA, Bonhoeffer T, Korte M (2005) The p75 neurotrophin receptor negatively modulates dendrite complexity and spine density in hippocampal neurons. J Neurosci 25:9989–9999.

Zhang XL, Pöschel B, Faul C, Upreti C, Stanton PK, Mundel P (2013) Essential role for synaptopodin in dendritic spine plasticity of the developing hippocampus. J Neurosci 33:12510–12518.